IMPACT OF DEFECTS ON THE MECHANICAL CHARACTERISTICS OF TWO-DIMENSIONAL NANOPOROUS BORON NITRIDE MEMBRANES

Van-Trung Pham[1]*, Thien-Kim Huynh[1], Le-Hung-Toan Do[1], Thi-Nhai Vu[2], Van-Thanh Hoang[1], Duc-Binh Luu[1]

[1]The University of Danang - University of Science and Technology, Vietnam
[2]Nha Trang University, Khanh Hoa Province, Vietnam

*Corresponding author: pvtrung@dut.udn.vn

(Received: April 05, 2025; Revised: June 15, 2025; Accepted: June 20, 2025)

DOI: 10.31130/ud-jst.2025.23(9C).535E

Abstract - This study investigates the effect of vacancy defects on the tensile properties of monolayer h-BN under uniaxial loading conditions, using molecular dynamics simulations. The analysis focuses on two key defect parameters: the length of the vacancy and the rotation angle of the defect with respect to the loading direction. The findings indicate that the frequency and extent of phase transition are influenced by the defect length and the direction of applied tension. Vacancy defects reduce rupture strain by causing stress concentrations that cause crack initiation at the defect region. As defect length increases in a direction perpendicular to the applied load, there is a noticeable reduction in Elastic modulus, maximum strength, and rupture strain, although no consistent trend is observed. Additionally, maintaining a constant defect size while changing the rotation angle (θ) reveals a similar pattern: increasing θ tends to reduce the Elastic modulus, maximum strength, and rupture strain.

Key words - h-BN; phase transition; vacancy defects; fracture strain; and molecular dynamics simulation

1. Introduction

Following the revolutionary breakthrough of graphene in 2004 [1], a significant amount of research has been carried out on various two-dimensional (2D) materials for numerous applications. Because of its adaptability in areas including biomaterials, electrocatalysis, photocatalysis, energy generation, and energy storage, 2D materials with adjustable nanopore sizes and shapes have attracted a lot of interest [2-4]. These porous materials possess the unique ability to interact with various active species, both within their internal frameworks and on their external surfaces. However, this interaction is highly dependent on the compatibility between the pore size and the size of the interacting species-an essential factor in applications such as adsorption, separation, gas storage, and heterogeneous catalysis [5-6]. Consequently, numerous fabrication techniques have been developed to create porous nanostructures that incorporate functional building blocks tailored to specific applications [7].

Hexagonal boron nitride (h-BN) is recognized as a highly promising two-dimensional (2D) material, owing to its outstanding mechanical strength, chemical, and thermal stability [8]. Structurally, single-layer h-BN resembles graphene, with a hexagonal lattice composed of alternating nitrogen and boron atoms rather than carbon. Due to this similarity, both materials have been considered ideal candidates for constructing heterostructures with tunable physical properties [9]. Although h-BN shares many desirable features with graphene, such as durability, chemical resistance, high thermal conductivity [10], it also exhibits unique traits. Notably, h-BN possesses intrinsic half-metallicity without requiring external electronic field modulation [11]. In previous research, Falin et al. [12] examined the indentation behavior of h-BN nanosheets and found that, unlike graphene, the mechanical strength of h-BN remains consistent even as the number of layer increases. This differs from graphene, where strength significantly decreases with added layers. Additionally, h-BN displays excellent ultraviolet optical properties [13] and offers advantages in various applications, including as a lubricant [14], a dielectric material for microwave absorption [15], a thermal conductor [16], and so on. These qualities have made h-BN an increasingly popular focus of nanomaterials research. Recent studies have further explored its mechanical and thermal performance. For example, Yang et al. [17] demonstrated stable crack propagation in monolayer h-BN, suggesting its potential as a protective material in 2D electronic devices. Other researchers have analyzed the mechanical properties of graphene and h–BN heterostructures [18], revealing new insights through combined molecular dynamics and theoretical models. These findings highlight the remarkable versatility of h-BN and its growing importance in nanoscience and technology.

As mentioned earlier, gaining a more comprehensive understanding of the relationship between structure and properties is essential for the design and optimization of materials in various engineering applications. Despite the promising potential of hexagonal boron nitride (h-BN), limited research has been conducted on the mechanical behavior of single-layer h-BN containing uniformly distributed vacancy defects. In particular, the effects of defect length and the rotation angle of these vacancies under uniaxial tensile loading have not been thoroughly explored. Therefore, further investigation is necessary to assess how these factors influence the mechanical performance of nanoporous 2D h-BN thin film.

2. Model and Method

The current investigation utilizes molecular dynamics simulations to determine how vacancy defects alter the mechanical characteristics of 2D h-BN membranes. A monolayer h-BN model was developed to investigate its behavior under uniaxial tensile loading, providing valuable insights into the material's load-bearing capacity. The simulations were conducted on h-BN structures with varying defect lengths and rotation angles, as illustrated in Figure 1. In order to remove interlayer interactions, a 5 nm vacuum space was added between the top and bottom of

the nanosheet along the Z-axis. The model's dimensions were fixed at 10.5 × 10.5 nm. Periodic boundary conditions were applied in all three spatial directions. Prior to tensile testing, the system was relaxed using the conjugate gradient (CG) minimization method to reach equilibrium.

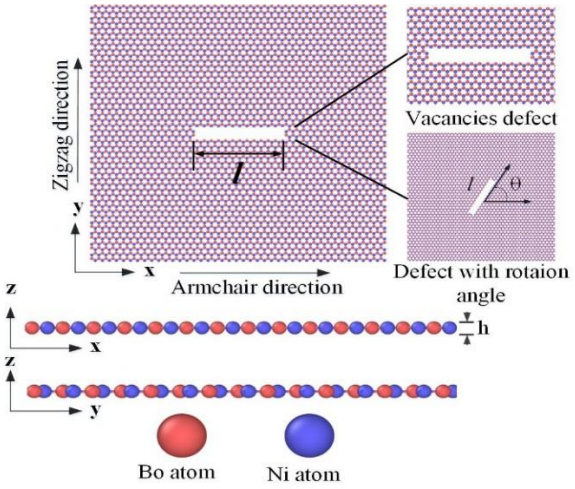

Figure 1. *Schematic illustration of h-BN nanosheet with variation in length and the rotation angle of defects at the nanosheet's center set up for the uniaxial tensions*

Two scenarios were identified from the vacancy defects at the central point of model: changes in the defect angle (θ) and variation of the defect lengths (l).

The interior stress was computed while applying tensile loading to assess h-BN membrane's mechanical properties. The virial theorem [19] can be utilized to define the stress component.

$$\sigma = \frac{1}{V}\sum_{a\in V}\left[-m_a v_a\theta \otimes v_a + \frac{1}{2}\sum_{a\neq b}(r_{ab}\otimes F_{ab})\right] \quad (1)$$

these settings in this equation, v_a and m_a represent the velocity vector and mass of atom a, respectively, whereas the spacing vector between particles a and b is denoted by r_{ab}. The volume of the simulation domain is indicated by the symbol V. The tensor product of two vectors is represented by the symbol ⊗. The force which particle b applies to particle a is denoted by F_{ab}.

The given equation provides the von Mises stress σ_{von} [20]:

$$\sigma_{von}^2 = \frac{1}{2}\begin{bmatrix}(\sigma_{xx}-\sigma_{yy})^2+(\sigma_{yy}-\sigma_{zz})^2\\ +(\sigma_{zz}-\sigma_{xx})^2+6(\sigma_{xy}^2+\sigma_{yz}^2+\sigma_{zx}^2)\end{bmatrix} \quad (2)$$

Every stress value is expressed in N/m. The strain is defined by the below equation:

$$\varepsilon = \frac{L-L_0}{L_0} \quad (3)$$

Assuming that L is the strained size of the structure, and L_0 is the initial size of the structure.

All molecular dynamics (MD) simulations in this study were carried out using the LAMMPS [21]. The Tersoff potential created by Kınacı et al. [22] was used to describe the atomic bonds within the single-layer h-BN membrane. This potential has been widely used in earlier research to simulate h-BN's behavior at the atomic scale. Visualization and post-processing of the simulation data were performed using OVITO software [23], which enabled detailed analysis of the structural and mechanical responses.

3. Results and discussion

3.1. Influence of vacancy defect length

This study starts by examining the fracture development of the monolayer h-BN nanosheet with varying vacancy defect lengths under axial tensile test along the x-direction at 300 K, as shown in Figure 2. The presence of vacancy defects significantly decreases the fracture strain of the nanosheets, as illustrated in Figure 2. However, there is no discernible or steady pattern in the associated rupture strain values as the length of the defect rises along the tension direction (x-direction). With defect lengths of 0 nm (perfect model), 1.1 nm, 2.1 nm, 3.2 nm, 4.2 nm, and 5.3 nm, cracks initiate at strain values of 32.50%, 19.49%, 26.60%, 28.07%, 29.06%, and 27.71%, respectively, as depicted in Figures 2(a2-f2). The results indicate that, in pristine membranes, stress is uniformly distributed across the material. In contrast, the presence of defects results in localized stress concentrations, leading to crack initiation, which then propagates rapidly in a direction perpendicular to the applied tensile load, specifically along the zigzag orientation, as illustrated in Figures 2(a3-f3). As the strain further increases, the cracks grow quickly until final rupture occurs at strain values of 32.65%, 21.01%, 26.73%, 28.18%, 29.16%, and 27.82%, respectively, as shown in Figures 2(a4-e4). This suggests that variations in vacancy defect lengths along the tensile path did not substantially alter the fracture strain when the defect width remained constant, and the results are also consistent with those reported in the earlier article [24]. The rupture spreads perpendicular to the strain orientation in every case with different vacancy defect lengths.

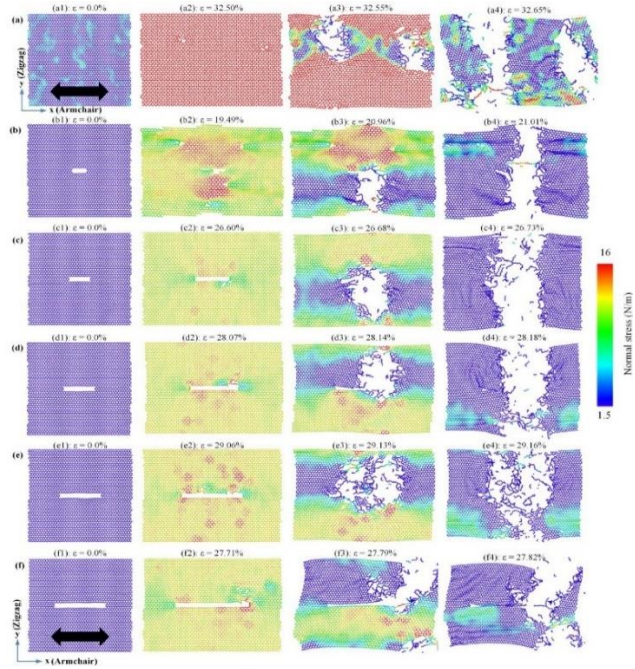

Figure 2. *The stress distribution and deformation evolution under uniaxial tension along the x (armchair) direction of h-BN membrane at 300K with various lengths of vacancy defects: (a) perfect model, (b) 1,1 nm, (c) 2,1 nm, (d) 3,2 nm, (e) 4,2 nm, (f) 5,3 nm*

Figure 3 illustrates single-layer h-BN nanosheet's fracture processes under axial tensile test along the y-direction at 300 K with various defect lengths. Tension in the y-orientation shows a significantly lower strain value than tension in the x-direction. The fracture strain does not exhibit a consistent pattern as the length of the vacancy defect, oriented perpendicular to the tension direction, rises. According to Figure 3(b-f), stress concentration on either sides of the flaw becomes apparent in all five scenarios as the defect starts to spread along the zigzag path. Stress distribution becomes more noticeable around the greater defect when the strain reaches values of 14.52%, 14.25%, 14.66%, 15.06%, and 14.55%, which starts the fracture process. At strain levels of 14.88%, 14.85%, 16.57%, 15.31%, and 16.32%, respectively, these faults subsequently spread quickly in a direction perpendicular to the tension until the nanosheet is completely broken. Under y (zigzag) tensile test, cracks with different defect lengths in h-BN sheets propagate perpendicular to the direction of strain, just like in the x (armchair) tension scenario.

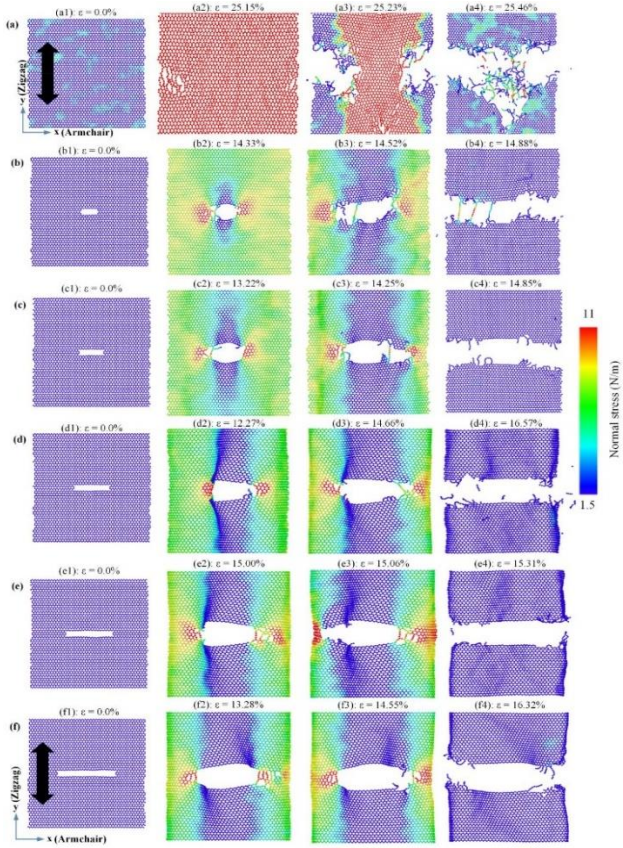

Figure 3. *The stress distribution and deformation evolution under uniaxial tension along the y (zigzag) direction of h-BN membrane at 300K with various lengths of vacancy defects:* ***(a)*** *perfect model,* ***(b)*** *1,1 nm,* ***(c)*** *2,1 nm,* ***(d)*** *3,2 nm,* ***(e)*** *4,2 nm,* ***(f)*** ***5****,3 nm*

Figures 4a and 4b illustrate the tensile stress-strain relationships of a single-layer h-BN sheet, subjected to uniaxial tensile tests along both the X (armchair) and Y (zigzag) orientations at 300 K. These plots demonstrate how varying defect lengths (while maintaining a consistent width of 0.4 nm) influence the material's mechanical response. Initially, the stress-strain curve shows a linear correlation at low strain levels. This is followed by a non-linear phase, which culminates in the ultimate stress before the membrane ruptures, indicated by a sudden drop in stress. Within this non-linear region, a phase transition may occur, with its extent and appearance being dependent on both the vacancy defect length and the direction of tensile loading. For example, Figure 4a reveals that for a membrane with a 1.1 nm defect length under uniaxial tension along the X (armchair) direction, the phase transition takes place between strain values of 11.49% and 19.49%. More comprehensive details concerning this membrane's phase transition are presented in Figure 6. For a membrane containing a vacancy defect of 5.3 nm, a noticeable phase transition is observed when the material is subjected to uniaxial tension in the armchair direction. Specifically, the transition occurs within a narrow strain range, between 27.71% and 27.73%, as illustrated in Figure 2f. Further insights into this phase change are provided in Figure 4a. Conversely, when the same membrane is stretched along the zigzag direction, phase transitions are found to be infrequent. This behavior is clearly demonstrated in Figure 3(a2-f2) and 4b.

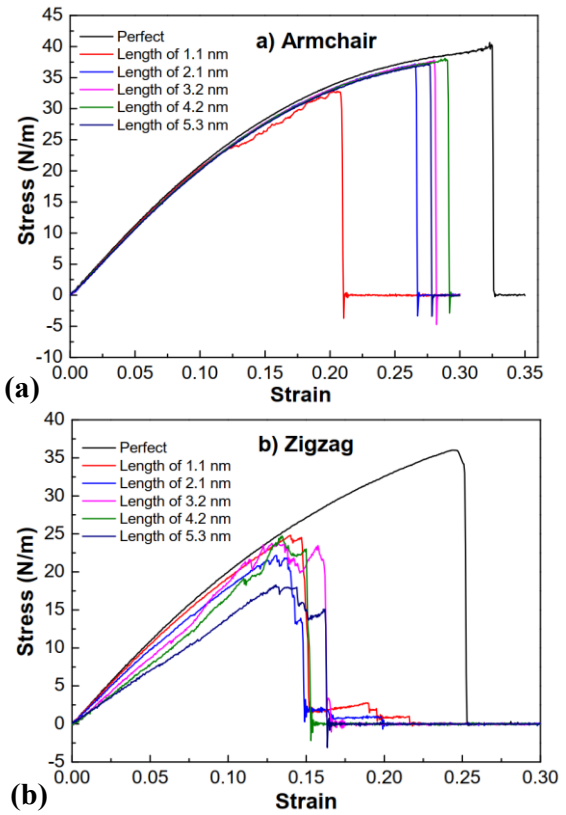

Figure 4. *Tensile stress-strain curves of the h-BN thin film at 300 K, θ = 0° with various in length while keep the same 0.4 nm in width of vacancy defects under uniaxial tensile along* ***(a)*** *the armchair direction and* ***(b)*** *the zigzag direction*

The defect length dependence of maximum strength is is derived from the stress–strain curves and is presented in Figure 5a. It shows that the pristine h-BN monolayer possesses the highest strength. However, once vacancy defects begin to appear in the membranes, their strength declines. Despite this reduction, there is no clear trend in strength as the defect length increases under uniaxial

tension. Additionally, considering the length of vacancy defects, the strength of h-BN sheets is greater when they are stretched in the X (armchair) orientation compared to when they are stretched in the Y (zigzag) orientation. The variation of Young's modulus with defect length is determined based on the stress–strain curves and illustrated in Figure 5b. Unlike the trend observed in strength, as the length of the flaw rises, Young's modulus consistently decreases. Additionally, elastic modulus under armchair tensile is found to be higher than that under zigzag tension. Based on the relationship between defect length and Young's modulus values of the h-BN membranes, this research derives a linear equation for Young's modulus E in relation to the defect length L as follows:

$$\text{X-path: } E = -2.10457L + 227.40 \text{ (N/m)} \quad (4)$$

$$\text{Y-path: } E = -16.8718T + 242.91 \text{ (N/m)} \quad (5)$$

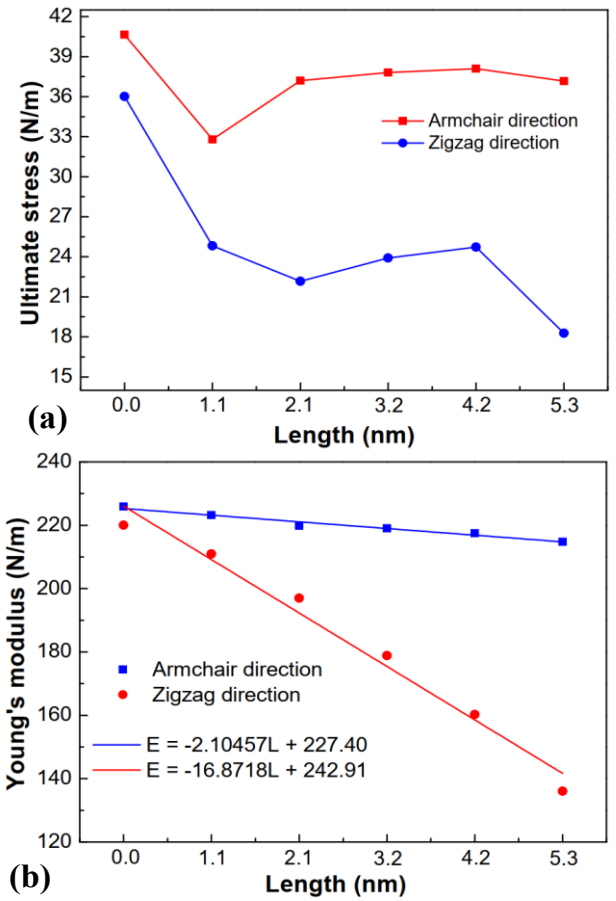

Figure 5. *(**a**) The ultimate stress as a function of vacancy defect length. (**b**) The Young's modulus of monolayer h-BN membrane at 300, θ = 0° for different lengths of vacancy defect compared to the perfect model under uniaxial tensile along the armchair and zigzag direction*

Figure 6 illustrates the phase transition of the h-BN membrane with a vacancy defect length of 1.1 nm under uniaxial tension in the X (armchair) orientation. According to the chart shown in the Figure 4a, the stress increases steadily with strain until it reaches 11.49%, at which point the membrane enters the inelastic deformation stage. At this strain level, the bond between atoms A and B reaches its critical threshold and begins to break, initiating a phase transition from a six-membered ring structure to a ten-membered ring, as shown in Figure 6(a-b). When the strain increases to 11.55%, the bond between atoms C and D also breaks, as illustrated in Figure 6c. As the strain continues to rise, the transformation from six-membered to ten-membered rings progresses further. Notably, this phase transition propagates along the zigzag edge, as depicted in Figure 6d. Eventually, this process leads the membrane to its critical limit, resulting in structural failure, as demonstrated in Figure 2b.

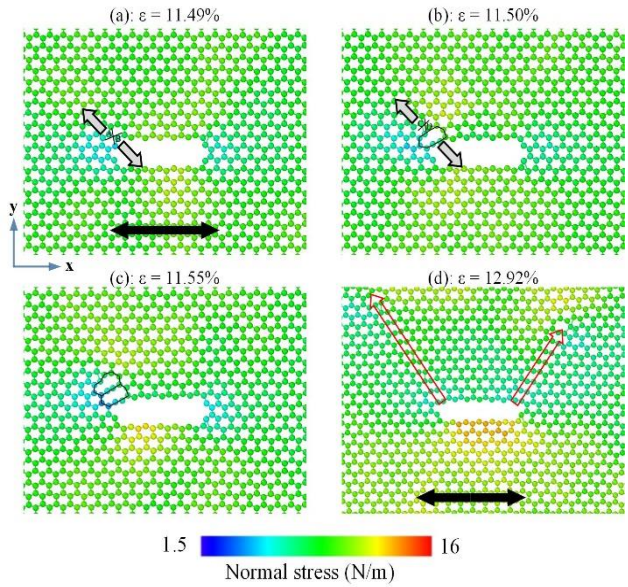

Figure 6. *Representative MD snapshots of hexagonal boron nitride (h-BN) with a length of 1.1 nm under varying strain percentages: **(a)** 11.49%, **(b)** 11.50%, **(c)** 11.55%, and **(d)** 12.92% (scale bar illustrates the magnitude of the normal stress, σxx)*

3.2. Influence of vacancy defect rotation angle

The impact of the flaw angles of rotation on the h-BN membrane's mechanical performance is investigated in this section. The flaw angles of rotation (abbreviated as θ) is the angle between the path of applied tension and the flaw edge when the membrane is under axial tensile test in both the armchair and zigzag orientations. The membrane's deformation behavior under axial tensile loading in the armchair configuration at 300 K is depicted in Figure 7, taking into account different defect rotation angles. The angle θ fluctuates from 0° to 90° while maintaining a consistent defect size of 3.2 nm for the defect length and 0.4 nm for the defect breadth. The membrane begins to crack at different strain levels depending on the angle: 28.07% (θ = 0°), 13.79% (15°), 14.65% (30°), 19.12% (45°), 11.65% (60°), 14.35% (75°), and 14.45% (90°). Complete failure occurs at corresponding strain values of 28.18%, 19.01%, 16.46%, 19.72%, 16.17%, 14.96%, and 19.44%, respectively. The path of crack propagation significantly varies as the flaw angles of rotation rises. At lower angles, the cracks appear rougher, whereas at higher angles, particularly at 75° and 90°, rifts propagate perpendicular to the loading orientation and tend to be sharper. However, despite these variations in crack behavior, the failure strain does not exhibit a clear or consistent trend with increasing rotation angle.

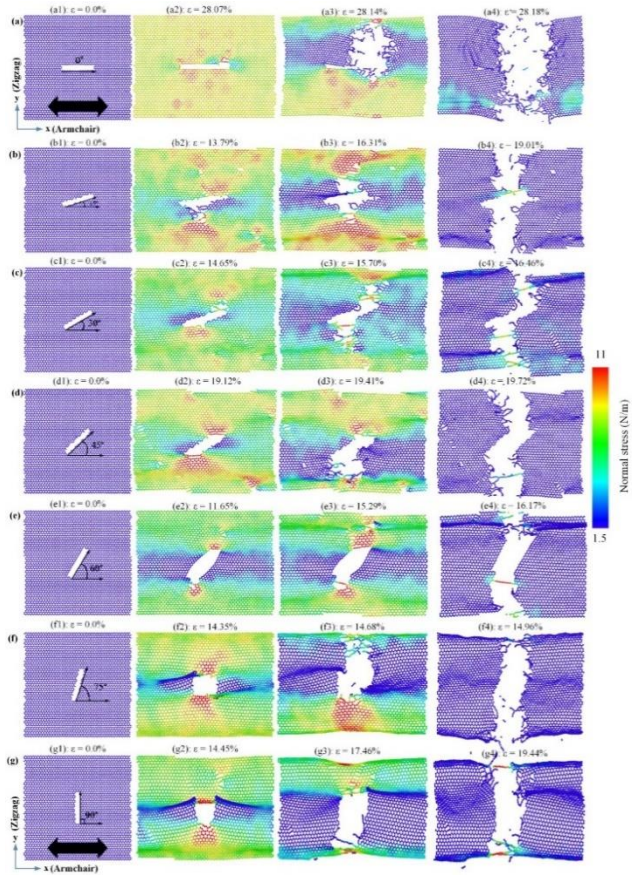

Figure 7. *The deformation behavior of an h-BN membrane subjected to uniaxial tension along the armchair orientation, with various defect rotation angles. These angles include* ***(a)*** *θ = 0°,* ***(b)*** *θ = 15°,* ***(c)*** *θ = 30°,* ***(d)*** *θ = 45°,* ***(e)*** *θ =60°,* ***(f)*** *θ = 75°,* ***(g)*** *θ = 90°*

The deformation and fracture behavior of a single-layer h-BN nanosheet, subjected to uniaxial tension along the zigzag (y-axis) at 300 K, is visually represented in Figure 8. The thin film contains vacancy defects that are fixed in size, measuring 3.2 nm in long and 0.4 nm in breadth. The defect angle θ, which is the angle between the loading direction and the defect edge, fluctuates from 0° to 90°. Similar to *x*-orientation case, particles under lofty stress tend to accumulate near the flaw region during tensile test, leading to early rupture of bonds in these regions. For rotation angles of 0°, 15°, 30°, 45°, 60°, 75°, and 90°, cracks begin to form when strain value obtains 28.07%, 17.17%, 16.32%, 13.88%, 12.56%, 17.56%, and 12.27%, respectively. In all defective membranes, the fracture propagates perpendicularly to the direction of the applied tension, following a pattern consistent with previous observations.

These results highlight a clear correlation between defect orientation and crack propagation, as well as noticeable variations in fracture strain depending on the rotation angle. Thus, the angle θ plays a significant role in influencing the mechanical response of the monolayer h-BN sheet under uniaxial loading.

Figure 9(a-b) present the stress–strain behavior of a monolayer h-BN membrane at 300 K under uniaxial tension along the armchair and zigzag directions, considering different rotation angles (θ) while keeping the defect size constant at 3.2 nm in length and 0.4 nm in breadth. The results show that changes in the rotation angle have a considerable impact on the membrane's mechanical performance. The mechanical qualities gradually deteriorate as flaw angle rises, with the peak strength being recorded at θ = 0°. This reduction in strength can be attributed to the geometric projection of the defect: as θ rises, the component of the flaw length perpendicular to the loading path becomes larger. As a result, the effective load-bearing region decreases, leading to greater stress concentration near the defect edge. Once the stress exceeds the bond strength at these critical points, crack initiation and propagation are facilitated, accelerating the failure process of the nanosheet. Despite this general trend of decreasing strength, the variation in fracture strain and ultimate stress with increasing θ does not follow a clearly consistent pattern.

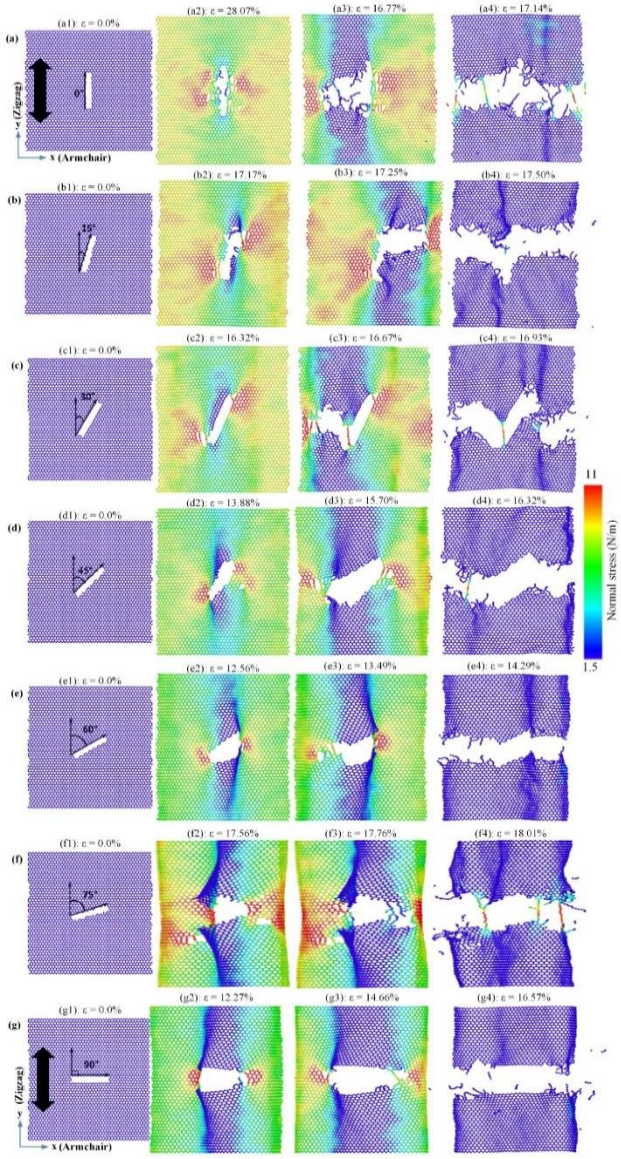

Figure 8. *The deformation behavior of an h-BN membrane under uniaxial tension along the zigzag orientation is presented for various defect rotation angles:* ***(a)*** *θ = 0°,* ***(b)*** *θ = 15°,* ***(c)*** *θ = 30°,* ***(d)*** *θ = 45°,* ***(e)*** *θ =60°,* ***(f)*** *θ = 75°,* ***(g)*** *θ = 90°*

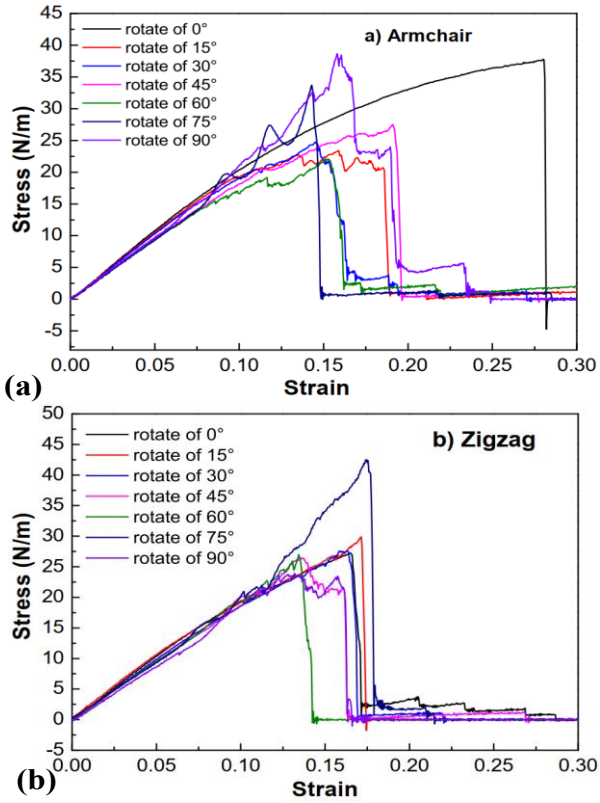

Figure 9. *The tensile stress-strain curves for the h-BN membrane at 300 K are presented, illustrating the effect of varying rotation angle (θ) while maintaining a constant defect size (3.2 nm length, 0.4 nm width). These curves show behavior under uniaxial tension applied along both (a) the armchair and (b) the zigzag directions*

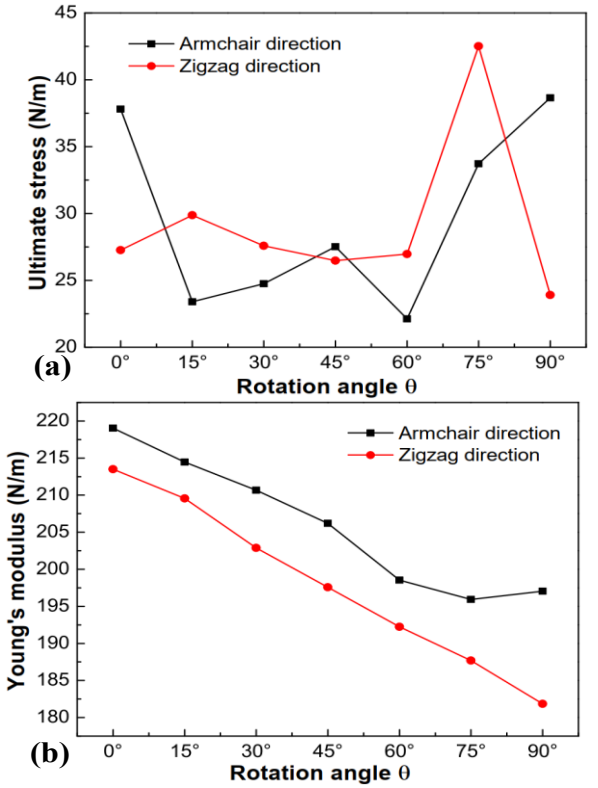

Figure 10. (a) *The rotation angle θ of vacancy defect dependence of ultimate stress.* ***(b)*** *The Young's modulus of monolayer h-BN membrane at 300, for different rotation angles θ of vacancy defects under both uniaxial tensile along the Armchair and zigzag directions*

The effect of the flaw angles of rotation on the Young's modulus and ultimate stress of monolayer h-BN membrane under uniaxial tension at 300 K is shown in Figure 10. The results clearly indicate that the rotation angle (θ) has a significant impact on the mechanical properties of the material. As θ increases, Young's modulus shows a decreasing trend under uniaxial loading. However, the ultimate stress does not exhibit a consistent pattern with the change in rotation angle. This behavior can be attributed to the increasing projection of the flaw edge in the orientation perpendicular to the applied tension. As a result, the effective load-bearing cross-sectional area is reduced, leading to higher stress concentration in localized regions. When this localized stress exceeds the critical bond strength, premature failure of the nanosheet occurs.

4. Conclusion

This study explores the impact of vacancy defects on the mechanical properties, distortion, and rupture behavior of two-dimensional hexagonal boron nitride (h-BN) membranes using molecular dynamics simulations under uniaxial tensile loading. By varying defect lengths and rotation angles in both x- and y-orientations, the analysis reveals that such defects significantly degrade the mechanical performance of h-BN. For example, the Young's modulus of a pristine membrane at 300 K is 225.88 N/m in the armchair and 220.07 N/m in the zigzag direction, while the introduction of defects leads to a marked reduction in stiffness, strength, and durability. As defect length increases perpendicular to the loading direction, Young's modulus, ultimate strength, and fracture strain consistently decrease, whereas changes in defect length along the loading direction show no clear trend. Similarly, increasing the defect rotation angle θ while keeping defect size constant results in reduced mechanical performance; however, variations along the tensile direction do not follow a clear pattern, and the highest strength is always observed at θ = 0°.

Additionally, at critical strain levels, atomic bonds-particularly between atoms A and B-begin to break, triggering a structural transformation from six-membered to ten-membered rings, with the occurrence and severity of this phase transition depending on both defect size and the direction of applied stress.

Acknowledgments: This research is funded by Ministry of Training and Education, Vietnam, under Project Number B2025.DNA.06.

REFERENCES

[1] K. S. Novoselov *et al.*, "Electric field effect in atomically thin carbon films", *Science*, vol. 306, no. 5696, pp. 666-669, 2004.

[2] H. Wang, X. Liu, P. Niu, S. Wang, J. Shi, and L. Li, "Porous two-dimensional materials for photocatalytic and electrocatalytic applications", *Matter*, vol. 2, no. 6, pp. 1377-1413, 2020.

[3] A. Mazinani *et al.*, "Comparative antibacterial activity of 2D materials coated on porous-titania", *Journal of Materials Chemistry B*, vol. 9, no. 32, pp. 6412-6424, 2021.

[4] J. S. Jang *et al.*, "2D materials decorated with ultrathin and porous graphene oxide for high stability and selective surface activity", *Advanced Materials*, vol. 32, no. 36, pp. 2002723, 2020.

[5] T. Liu, J. Ding, Z. Su, and G. Wei, "Porous two-dimensional materials for energy applications: Innovations and challenges", *Materials Today Energy*, vol. 6, pp. 79-95, 2017.

[6] M. H. Sun *et al.*, "Applications of hierarchically structured porous materials from energy storage and conversion, catalysis, photocatalysis, adsorption, separation, and sensing to biomedicine", *Chemical society reviews*, vol. 45, no. 12, pp. 3479-3563, 2016.

[7] M. L. K. Hoa, M. Lu, and Y. Zhang, "Preparation of porous materials with ordered hole structure", *Advances in colloid and interface science*, vol. 121, pp. 9-23, 2006.

[8] L. Boldrin, F. Scarpa, R. Chowdhury, and S. Adhikari, "Effective mechanical properties of hexagonal boron nitride nanosheets", *Nanotechnology*, vol. 22, no. 50, pp. 505702, 2011.

[9] M. P. Levendorf, C. J. Kim, L. Brown, P. Y. Huang, R. W. Havener, D. A. Muller, and J. Park, "Graphene and boron nitride lateral heterostructures for atomically thin circuitry", *Nature*, vol. 488(7413), pp. 627-632, 2012.

[10] C. Li, Y. Bando, C. Zhi, Y. Huang, and D. Golberg, "Thickness-dependent bending modulus of hexagonal boron nitride nanosheets", *Nanotechnology*, vol. 20, no. 38, pp. 1-10, 2009.

[11] F. Zheng *et al.*, "Half metallicity along the edge of zigzag boron nitride nanoribbons", *Physical Review B-Condensed Matter and Materials Physics*, vol. 78, no. 20, pp. 205415, 2008.

[12] A. Falin *et al.*, "Mechanical properties of atomically thin boron nitride and the role of interlayer interactions", *Nature communications*, vol. 8, no. 1, pp. 15815, 2017.

[13] K. Watanabe, T. Taniguchi, and H. Kanda, "Direct-bandgap properties and evidence for ultraviolet lasing of hexagonal boron nitride single crystal", *Nature materials*, vol. 3, no. 6, pp. 404-409, 2004.

[14] Y. Bai *et al.*, "Ball milling of hexagonal boron nitride microflakes in ammonia fluoride solution gives fluorinated nanosheets that serve as effective water-dispersible lubricant additives", *ACS Applied Nano Materials*, vol. 2, no. 5, pp. 3187-3195, 2019.

[15] M. Wang *et al.*, "Facile fabrication of Hildewintera-colademonis-like hexagonal boron nitride/carbon nanotube composite having light weight and enhanced microwave absorption", *Journal of Colloid and Interface Science*, vol. 564, pp. 454-466, 2020.

[16] L. An, N. Zhang, X. Zeng, B. Zhong, and Y. Yu, "Quasi-isotropically thermoconductive, antiwear and insulating hierarchically assembled hexagonal boron nitride nanosheet/epoxy composites for efficient microelectronic cooling", *Journal of Colloid and Interface Science*, vol. 608, pp. 1907-1918, 2022.

[17] Y. Yang *et al.*, "Intrinsic toughening and stable crack propagation in hexagonal boron nitride", *Nature*, vol. 594, no. 7861, pp. 57-61, 2021.

[18] Y. Li, A. Wei, H. Ye, and H. Yao, "Mechanical and thermal properties of grain boundary in a planar heterostructure of graphene and hexagonal boron nitride", *Nanoscale*, vol. 10, no. 7, pp. 3497-3508, 2018.

[19] D. Wang, J. Lee, K. Holland, T. Bibby, S. Beaudoin, and T. Cale, "Von mises stress in chemical-mechanical polishing processes", *Journal of the Electrochemical Society*, vol. 144, no. 3, pp.1121, 1997.

[20] M. Asgari, and M. A. Kouchakzadeh, "An improved plane strain/plane stress peridynamic formulation of the elastic–plastic constitutive law for von Mises materials", *Engineering with Computers*, vol. 40, no. 4, pp. 2127-2142, 2024.

[21] S. Plimpton, "Fast parallel algorithms for short-range molecular dynamics", *Journal of Computational Physics*, vol. 117, no. 1, pp. 1-19, 1995.

[22] A. Kınacı, J. B. Haskins, C. Sevik, and T. Çağın, "Thermal conductivity of BN-C nanostructures", *Physical Review B-Condensed Matter and Materials Physics*, vol. 86, no. 11, pp. 115410, 2012.

[23] A. Stukowski, "Visualization and analysis of atomistic simulation data with OVITO–the Open Visualization Tool", *Modelling and simulation in materials science and engineering*, vol. 18, no.1, pp. 015012, 2009.

[24] V. T. Pham, T. K. Huynh, and T. N. Vu, "Effect of defect on mechanical properties of two-dimensional MoS2 membranes", *Physica Scripta*, vol. 100, no. 4, pp. 045407, 2025.